THE MOMENTUM DISTRIBUTION OF CHARGED COSMIC RAY PARTICLES NEAR SEA LEVEL

Thesis by

Donald Arthur Glaser

In Partial Fulfillment of the Requirements

For the Degree of

Doctor of Philosophy

California Institute of Technology

Pasadena, California

1950

ACKNOWLEDGEMENTS

The results reported here represent the culmination of the work of several people. Drs. B. Hamermesh and R. B. Leighton designed and built much of the apparatus. Dr. G. Safonov helped complete and perfect the instrument and made a preliminary run of 330 pictures. Mrs. C. D. Strauss and Mr. C. W. Faessler assisted in making the measurements and in reducing the data.

Finally the author would like to express his gratitude to Professor C. D. Anderson, who suggested that the experiment be done in its present form, for his constant encouragement and guidance.

ABSTRACT

A new measurement of the momentum distribution of high energy charged cosmic ray particles at sea level has been made by means of a technique involving the use of two cloud chambers and a large electromagnet. With about twice the precision of previous determinations, the spectrum is extended to a momentum of pc = 80 Bev. For the 1547 measureable sets of tracks recorded, the positive-negative ratio is 1.26 ± 0.06. Up to the highest momenta measured the differential spectrum falls off as $1/p^s$ with s = 2 very nearly. The positive excess and positive-negative ratio appear to be functions of momentum with the positives predominating at about 1.3 Bev. In other respects the positive and negative spectra are very similar.

Although the effect is barely outside statistical uncertainty, there seems to be an anomolous dip in the momentum distribution at about 3 Bev. In addition to this there seems to have been a small diurnal variation in the spectrum during the time the experiments were performed, 1 Bev and 4 Bev particles being slightly favored during the day and 3 Bev and 7 Bev particles being favored at night. These effects are discussed and the present results are compared with data of other experimenters.

TABLE OF CONTENTS

CHAPTER I

Introduction

One of the remarkable and striking properties of the cosmic radiation is its extraordinarily great penetrating power. Early experiments soon demonstrated that the most penetrating component of cosmic rays must consist mainly of charged particles, mesons and protons, rather than of very energetic photons. Using theoretical expressions for the energy loss of these particles in traversing matter, it is possible to estimate their energies from the results of absorption measurements. Such estimates indicate that the particles have energies up to 10^{12} ev and possibly higher. If the very large air showers are initiated by single particles, they furnish evidence of the existence of particles of 10^{16} ev of energy or more in the cosmic rays. Particles emitted by naturally and artifically radiactive materials, by nuclear fission, and from various types of particle accelerators all have energies less than several hundreds of Mev so that much of the interest in the study of cosmic rays has centered on the discovery of the mechanism of production of such energetic particles and on the nature of interactions between particles that move so fast. A useful piece of information in these studies is the energy or momentum distribution of the cosmic ray particles. Three different methods have been used to attempt a measurement of this distribution for the charged cosmic ray particles.

There have been several unsuccessful attempts to determine the momentum distribution by measuring the deflections

of particles which have travelled through a strong magnet, using arrays of geiger counters to observe deflection angles. To date the only result of such experiments has been a determination of the ratio of the numbers of positive and negative particles in certain momentum ranges.

Another method for investigating the momentum distribution, or "momentum spectrum", depends on the absorption of the particles. From a plot of the intensity of radiation as a function of absorber thickness the momentum distribution of particles incident on the top of the absorber is calculated by means of the fairly well-known relation between range and momentum for cosmic ray particles. To carry out this calculation it is necessary to know the mass, charge, and spin of the particles concerned because the rate of energy loss due to ionization, radiation, and pair production depends on these characteristics of the particles. It is usually assumed that very nearly all of the charged particles of energy 0.5 Bev or more are mu mesons of mass about 216 electron masses, charge plus or minus one electronic charge, spin 1/2. Very few electrons have such a high energy because of the very great probability that they will degrade their energy in shower production. More detailed arguments and experimental evidence to support the above assumption will be given in what follows.

Absorption measurements of the momentum spectrum can be extended to very great energies by using sufficiently thick absorbers; experiments have been made underground to depths

of 1400 meters water equivalent. By one meter of water equivalent of a material we mean simply a thickness of 100 g/cm^2 according to current usage.

The most direct method of measuring the momentum spectrum of the cosmic rays, and the one which has given the most detailed information in its range of applicability, is the measurement of the curvatures of the tracks of a number of particles in a cloud chamber which is immersed in a uniform magnetic field. Several determinations have been made in this way up to about 10 Bev. Since we shall be interested here in particles of relativistic energy it is convenient to speak of the momentum in electron volts or Mev or Bev since the momentum is so nearly equal to the energy anyway. Strictly, we shall use p to denote the momentum times the velocity of light and put it in ev units. Detailed results of the various magnetic deflection experiments will be given later. All of them agree in the gross features of the distribution; a rise at the low end to a maximum at about 1 Bev and then a falling off roughly as the inverse square of the momentum out to 10 Bev.

The experiment described here is an extension of the magnetic deflection method to higher momenta and to higher accuracy in the range already investigated. Two cloud chambers are used, one placed above and the other below a region of fairly strong and uniform magnetic field. Straight tracks are observed and the angular deflection of the particle in tra-

versing the field is obtained from stereographic pictures which give the angle between the tracks. Although the double cloud chamber method is more difficult experimentally than the conventional single cloud chamber technique, it has several advantages which seem to make the added trouble worthwhile.

One of the most serious limitations on cloud chamber momentum measurements is distortion of the tracks by convection in the chamber gas. Much of this undesired motion is caused by temperature gradients resulting from the heat dissipated by the electromagnet which provides the magnetic field. Chambers mounted outside and away from the magnet are easier to insulate and hence cure this trouble. When the chambers are out of the magnetic field, the gap can be smaller so that the required field can be obtained more economically. In this experiment it is easy to judge the degree and nature of distortions as well as errors introduced by scattering in the gas of the cloud chamber since the tracks are expected to be perfectly straight and deviations from straightness are easy to evaluate objectively. We have introduced a new source of uncertainty, however; scattering in the material separating the sensitive volumes of the two chambers. It turns out that the effect of scattering on the spectrum is not serious as will be shown by a simple calculation which has been checked experimentally. A final advantage of the present method is the ease and accuracy with which the deflection angle can be measured as compared with the difficult task of measuring curvatures directly.

CHAPTER II

The Apparatus and Its Operation

The experiments described here were performed in Room 360 on the third floor of the west wing of The Norman Bridge Laboratory of Physics in Pasadena at an elevation of about 800 feet above sea level. All of the particles recorded here entered the apparatus from a nearly vertical direction after passing through a roof of duraluminum about two mm thick which constituted the only solid material above the top counter. The magnetic field was oriented nearly north and south and was horizontal. Data included in this survey were recorded between May 27 and September 9, 1949, during which time the apparatus was operated continuously day and night except when repairs and adjustments were necessary. Pictures were taken at the rate of six or seven an hour during normal operation. Fig. 1a shows the arrangement of the chambers and magnet without the box used for thermal insulation. In Fig. 1b the shaft cut through the laboratory roof can be seen. Its upper end is covered with the thin duraluminum sheet.

The Magnet

The electromagnet used in this experiment was constructed of 1500 pounds of 3-inch steel boiler plate energized by eight coils of copper wire of about 390 turns each. Each coil has a resistance of about 1 ohm at 20° C and is cooled by water flowing through 1/8-inch copper tubing soldered to copper sheets which cover the coils inside and out. It has a gap

1 1/4 inches long, 6 inches wide, and 16 inches high. During operation the magnet was protected by a current circuit breaker with selenium rectifiers to prevent arcing through the insulation when the circuit is broken, a water flow rate switch, a water pressure switch, a water thermoswitch, and a bridge circuit that turns off the current in the magnet if the voltage drops in the eight coils become seriously unequal. Current in the range 50 to 150 amperes was provided by a motor generator set with current regulation to about 2%. Cooling water flows through the magnet at the rate of about 0.3 liters/sec and is heated from 24°C to 27°C when 75 amps at 43 volts are supplied to the windings.

To calibrate and plot the magnetic field a flip coil of 30 turns of No. 36 enamelled wire wound on a spool of lucite 0.70 inches in diameter was used with a new Leeds and Northrup wall-type ballistic galvanometer. The coil was mounted so it could be flipped quickly through 180° by a spring when in the gap in the magnet and also inside various standard solenoids. Several methods were used to calibrate this measuring device.

In the first method the flip coil was operated at the center of a large air core solenoid whose field was very accurately known from previous calibrations in the course of a determination of e/m for the electron by the Zeeman effect (1). Using an ammeter calibrated in the electrical standards laboratory to 0.5% the standard solenoid was run at about 80 amperes to give calibration points for the flip coil and

galvanometer in the vicinity of 4 cm deflection. These measurements yield a galvanometer constant of 601 ± 6 gauss/cm.

A second measurement was made by measuring the field of a magnetron magnet with the test coil and with a fluxmeter provided with the magnet. From this determination the constant is 621 ± 12 gauss/cm in the neighborhood of 5 cm deflection. Because of the inhomogeneity of the magnetic field of this magnet, this constant is expected to be somewhat high since the fluxmeter coil is smaller than our flip coil.

For the third calibration a Rawson Fluxmeter was used with the same magnetron magnet. Deflections near 5 cm yielded a constant of 607 ± 12 gauss/cm.

The fourth calibration was carried out using a Hibbert Magnetic Flux Standard calibrated in the laboratory of Professor S. J. Barnett to about 0.1% using various standard solenoids. This instrument can be used to introduce a known number of flux linkages into a circuit by dropping various standard coils through the magnetostatic field of a very stable permanent magnet. Results of this calibration give 595 ± 10 gauss/cm in the range 5 cm to 10 cm and 588 ± 10 gauss/cm from 15 cm to 20 cm, the discrepancy being due to non-linearity of the galvanometer. From all these calibrations the best calibration was taken as 590 + (11/15)(20-D) gauss/cm where D is the deflection in cm. Although the correction for non-linearity is small, its effect might be felt in regions of weaker field.

A plot of the shape of the field showed it to be uniform to about 0.5% inside the gap, falling about 2% at a distance

1/2 inch from the boundaries and falling to 1/2 its maximum value 1 inch outside the gap. Hysteresis effects are completely negligible. As will be shown later, the quantity characterizing the magnetic field which is relevant in this experiment is the line integral $\int Bdl$, taken along a vertical straight line perpendicular to the field at the center of the gap. This integral was evaluated by measuring the area under a full size plot of the magnetic field intensity as measured with the flip coil. All of the tracks reported here were taken at 75 amperes magnet current which gives a value of 3.87×10^5 gauss-cm ± 2% for the integral described above.

The Cloud Chambers

As shown in Fig. 2a the cloud chambers are circular cylinders with pyrex glass walls 1/4 inch thick and a pyrex glass front plate 5/8 inch thick. The sensitive volume is 30 cm in diameter and 13 cm deep. An aluminum piston sealed to the sensitive volume by a 1/16-inch thick gum rubber diaphragm provides the volume expansion by moving through 5/8 inch to give an expansion ratio of about 1.12. The chambers were filled with argon and the vapor of a mixture of ethyl alcohol and water to a total pressure of about 8.5 pounds per square inch. It was found that the smallest expansion ratio could be used with a mixture containing 35% water by volume, and that the droplets grow somewhat faster for this combination than for pure ethyl alcohol. Expansion is achieved by discharging a 23-mfd condenser charged to 1000 volts through a solenoid which actuates a latch

mechanism and permits the piston to move back under the 95-pound force of the excess pressure of the chamber gas. Resetting is accomplished by admitting air at 20 pounds per square inch behind the piston to force it into the cocked position in which the latch holds it ready for the next expansion. Just in front of the piston is mounted an aluminum plate in which a large number of holes have been drilled along the chamber axis to help reduce turbulence in the chamber gas during the expansion. The plate is covered with black chiffon velvet which serves as a background for photography and also aids in reducing turbulence.

An electrostatic sweep field to reduce the number of free ions in the chamber gas is maintained by keeping a semiconducting aquadag ring painted on the inside of the chamber wall at 120 volts positive potential with respect to the grounded metal frame of the chamber. As soon as the chamber tripping cycle is initiated a 2051-type thyratron turns off the sweep field.

In order to allow successful continuous operation of the chambers without requiring constant adjustment of the expansion ratio, it was found necessary to air-condition the laboratory. The room was maintained at 23.4 ± 0.2°C by means of an evaporative cooler and thermostat arrangement.

Recording Technique

Each chamber is photographed stereographically to record the tracks by means of two cameras placed about 140 cm in front of the chamber, one of which looks along the chamber

axis, the other being parallel to the first but displaced 25 cm to the side. A 6-foot length of 1-mil tungsten wire is stretched vertically the whole length of the apparatus just in front of the cloud chamber to provide a reference direction with respect to which angles may be measured on the films. By using the very fast, high contrast, Eastman Kodak 35-mm Linagraph Panchromatic Recording Negative it is possible to operate the 10-cm Kodak Ektar lenses at f/8. Such a small stop opening results in sufficient depth of field to get sharp images of both the tracks and the reference wire just in front of the chambers.

To estimate the magnitude of distortions that might be introduced by the photographic process due to lens distortions, optical distortion by the front glass plate of the chambers, change of dimensions of emulsion during processing, and so on, a set of pictures of sheets of graph paper mounted on a plane surface inside the chamber were taken with the lenses wide open at f/4.5. No curvature or other distortion could be detected in the reprojected images by methods of the precision used to make measurements on the tracks in this experiment. For maximum contrast the film was developed for 12 minutes in Kodak D-19 developer at about 72°F.

Since the chambers were illuminated from the side as shown in Fig. 1 the light entering the cameras had to be scattered through 90° by the condensed droplets. It was necessary to use a very intense light source in order to get good pictures since the scattering at 90° by small droplets

is very small. A General Electric FT 422 xenon-filled flash tube was used with a set of three glass condensing lenses, each five inches in diameter and having a 5-inch focal length. The energy for each flash was provided by a 450-mfd bank of condensers charged to 2000 volts. A pulse transformer triggered the lamps with a 20,000-volt tickle pulse which initiated the discharge. No shutter was used on the cameras; they were left constantly open and the exposure was determined by the duration of the flash, which was about 3000 microseconds. The lights were tripped by a delay circuit whose cycle was initiated by the throwing of the tripping latch on the chambers. In this way the picture was taken at any desired time interval after the expansion. It is necessary to wait until the droplets have grown large enough to photograph although the sooner the picture is taken the smaller will be the distortions due to gas convection in the chamber.

Several seconds after the picture is taken a pulse of compressed air winds the film in the four cameras and advances the two frame counters which indicate the picture number in the photographs. Fig. 3 shows the four cameras and their mounting together with the chambers and magnet assembly.

The Geiger-Muller Counters

Two Geiger-Muller counters are used in a two-channel coincidence circuit to trip the chambers and initiate the whole cycle of the equipment. The counters are made of 20-gauge oxygen-free copper tubing 1 1/4 inches in diameter and about 7 1/2 inches long. Stupakoff glass to covar seals

support the center wire which is 1-mil tungsten. The counters are filled with argon to about 8 cm of mercury and petroleum ether vapor to another 1 cm of mercury. They are operated at about 1000 volts and have a plateau from 900 volts to 1200 volts. Their sensitive length is very nearly 6 inches.

The counters are placed one above the top chamber and the other below the bottom one in such a way that only a particle passing through the uniform portion of the field and the centers of the cloud chambers trip the apparatus, except, of course, for scattered particles and accidental coincidences.

Electrical Circuits

Although the geiger counters are of the self-quenching type they are operated with a multivibrator quench circuit which prolongs their life somewhat. In other respects the coincidence circuit is of the conventional type and has a resolving time of about 1 microsecond. The chambers are tripped when the firing of an OA5 gas-filled relay tube permits the discharge of a 23-mfd condenser at 1000 volts through a solenoid which operates the latch mechanism. At the same time a 2051-type thyratron turns off the sweep field.

As each latch is thrown it actuates a microswitch which causes a high voltage tickle pulse to fire the flashlamp which is maintained at 2000 volts across its condenser bank. A multivibrator delay circuit provides the 55-millisecond time required for the droplets to grow before the light is flashed and the picture taken. The cabinet housing the electronic controls is shown in Fig. 4.

Cycle of Operations

The following scheme represents the cycle of operations of the apparatus from the time a particle passes through it to the time it is ready to record the next such event. Most of the times involved have been measured fairly closely although some of the circuit times are not so well known.

Time	
0	geiger tubes record two counts separated by less than 2 microseconds
3 microseconds	OA5's fire and start discharge through solenoids that trip the cloud chambers, sweep fields go off
1 millisecond	plungers of trip solenoids reach the end of their travel and actuate light and recycling microswitches
10 milliseconds	expansion of chambers complete
55 milliseconds	lamps flash
3 seconds	compressed air pulse actuates air pistons which advance camera film and frame number indicators
10 seconds	sweep fields turned on
25 seconds	bottom chamber resets
35 seconds	top chamber resets
3 minutes	OA5 grids reconnected by relay; apparatus ready for next count

CHAPTER III

Theory of the Method

The purpose of this experiment is to determine the distribution function, I(p), in particles per unit momentum interval which pass through one square cm in a second per unit solid angle near the vertical in the natural cosmic radiation near sea level. We actually measure the counting rate, R(p), of the apparatus described in particles per second per unit momentum interval. R(p) is related to I(p) by the expression $R(p) = \iint I(p)d\Omega\, ds$ where the integral in $d\Omega$ is taken over the solid angle accessible to particles passing through a given ds and the integral in ds is taken over the area of the top geiger counter. The accessible solid angle is determined by the bottom counter and by the bending of the trajectory due to the magnetic field. To calculate its value and evaluate the above integral, we must consider the nature of the method used here to measure the momentum of a particle.

Momentum Determination

To an approximation sufficient for this experiment, the magnetic field used here can be considered to be a sharply bounded region of uniform field except for its variation in the vertical direction. Particles which get into the boundary regions in the horizontal direction are quickly lost from the field. Those few which do get bent back into the field can be discarded on the basis of an examination of their full scale reprojections from their positions and directions in the chambers.

The equation of motion of a particle carrying a single positive or negative electronic charge and moving in a plane perpendicular to a magnetic field of flux density B is

$$p = 3 \times 10^{-4} B(y) \rho(y'', y') \qquad (1)$$

if y is distance in cm measured in the direction in which the field varies, ρ is the radius of curvature of the path in cm, B is the magnetic induction in gauss, y' and y'' are derivatives with respect to x taken in the plane of motion perpendicular to y, and p is the momentum in Mev (we have agreed to use p for pc throughout). If ds is arc length along the path and φ is the angle between the path and the y axis

$$\rho = ds/d\varphi = dy/(\cos\varphi \; d\varphi) \qquad (2)$$

Since p is a constant of the motion we can substitute (2) into (1) and integrate

$$\int_{\varphi_1}^{\varphi_2} p \cos\varphi \; d\varphi = 3 \times 10^{-4} \int_{y_1}^{y_2} B(y)dy \qquad (3)$$

so that

$$p = 3 \times 10^{-4} \int_{y_1}^{y_2} B(y)dy \quad /(\sin\varphi_2 - \sin\varphi_1) \qquad (4)$$

Hence the momentum of the particle is determined by a vertical line integral of the magnetic induction and the angles of entry and exit at certain points in the field. The integral is evaluated from a plot of the magnetic field in the region between the two chambers including the region of fringing. Inside the chambers the field is too weak to cause observable deflection.

If the particle does not move in a plane perpendicular to the field this argument applies to the perpendicular component. For the counter geometry used here, the total can differ from the perpendicular component by only 0.02%. Also the geometry allows the sines to be replaced by their arguments to within 1%.

Effective Aperture of the Instrument

In the absence of a magnetic field the solid angle in which a given point on the top counter will accept particles depends on the size and position of the bottom counter only. For the two counters used here the integrated aperture of the instrument summed over the top counter is 0.0822 cm^2-steradians. Due to the magnetic field, the particles move in curved trajectories so that the limiting paths are different from those found without the field in such a way that the effective solid angle of the instrument is reduced. A simple and straightforward though somewhat tedious calculation has been made to evaluate the amount of this effect. An outline of the calculation has already been given in some detail (2). At 3 Bev and above the solid angle is within 1% of the no-field value. Below this momentum one must apply a correction to the observed momentum distribution to obtain the true distribution. At 2.4 Bev one must add 3%, at 1.5 Bev, 10%, at 1.0 Bev, 24%, and at 0.7 Bev, 60% must be added to the observed distribution. Particles of momentum less than about 0.3 Bev cannot trip the apparatus.

Determination of Particle Momenta from the Photographs

In a uniform magnetic field a charged particle of constant speed moves in a helical path, the pitch angle of the helix being the angle whose tangent is the ratio of the longitudinal to the transverse components of the momentum of the particle with respect to the field. The radius of the circular cylinder containing the helix is the radius of the circular path that would be followed by a particle moving perpendicular to the field with a momentum equal to the transverse momentum of the original particle. In the present experiment we have a very nearly uniform field with a small boundary region. The pitch angles of the helices of motion are limited by the counters to be less than about 0.02 radians and the angular portion of a turn is less than 0.4 radians. Our photographs represent the straight line tangents to these helices. We want to determine from them the angles of entry and exit of the particle projected onto a plane perpendicular to the magnetic field. To do this we take two photographs of each chamber, one with a camera looking directly down the axis of the chamber, the other using a camera parallel to the first, displaced 25 cm to the side. A detailed analysis of the geometrical relations needed to calculate the angles of interest from the measured ones has already been presented(2). We give here only the results and some modifications derived in a similar way.

Let φ be the angle on the film between the image of the track, and the vertical guide wire in the direct view of the

top chamber and φ_2 the corresponding angle in the side top view. Use φ_1' and φ_2' for the bottom chambers. Call the horizontal distance from the axis of the central camera to the track b for the upper and b' for the lower chamber. L is the distance from the front nodal point of the lens to the track, f, the distance from the rear nodal point to the film, and d, the separation of the two camera for each chamber. φ and φ' are the desired projected angles. Then

$$\varphi = \varphi_1 - \tan^{-1}\left[\frac{b \cos\varphi_1}{d \cos\varphi_2} \sin(\varphi_1 - \varphi_2)\right] \qquad (5)$$

where b is taken positive to the right of center in the chamber and φ is taken positive for tracks going up to the right as one looks at the chamber from the camera.

Angles are measured by projecting the images of the tracks onto a flat horizontal screen containing a grid of parallel lines. The screen is rotated about a vertical axis until the image of the track is parallel to the grid and again until it is parallel to the image of the wire. A circle of one meter radius with center at the axis of rotation moves with the grid and is used to read the angular position of the grid by means of a linear scale which allows measurement to the nearest tenth of a millimeter. The least count of the angular measuring device is thus 0.0001 radians. The distance b is measured directly in cm on this full size projection. Fig. 2b shows the full scale projection arrangement with the position of the counters and magnet indicated.

Since we are using here a small part of a very nearly

helical path, the tangents considered can be taken to be coplanar. Under this assumption one needs the data from only three of the cameras to determine the momentum. The pitch angle of the helix is very nearly the angle between the film plane and a plane containing the tracks and having a horizontal intersection with the film plane. This plane, which is very closely the osculating plane of the helix at the midpoint of the curved section of the trajectory, can be considered to be the plane of the path of the particle. If we call this angle β, equation (5) simplifies to

$$\tan \varphi = \tan \varphi_1 - \frac{b}{L} \tan \beta \qquad (6)$$

where we take β positive if the particle moves away from the cameras as it goes downward through the apparatus. When all four views are available, this 3-camera formula can be used to make certain that the particle has not been scattered, for then the values of β above and below might be unequal. If only three views are available, it allows calculation of the momentum with only those three. Because of the geometry of the counters and cameras, the stereoscopic correction term does not exceed 0.0015 radians which is less than 15% for particles of momentum less than 10 Bev. Only for particles of higher momentum than this is it necessary to use the stereoscopic correction. The quantity β is given in terms of b, φ_1, and φ_2 by the relation

$$\tan \beta = \frac{L_1 \cos \varphi_1}{d \cos \varphi_2} \left(\sin (\varphi_1 - \varphi_2)\right) \qquad (7)$$

Effects of Scattering on the Momentum Distribution

In addition to the magnetic deflections on which this experiment is based, the charged particles observed will suffer various amounts of angular deviation due to scattering by the walls of the cloud chambers and the gas in the space between the chambers. To evaluate the validity of the results obtained here, it is necessary to make some estimate of the effects of the scattering on the various characteristics of the distribution we are seeking to determine. We shall be interested in a change of the general shape of the distribution, the possible changes in the position of the maximum, the values of the exponent of the $1/p^n$ decrease at the high end, and finally, the modifications in any maxima or minima or "fine structure" that might be present.

In order to make our estimate we assume all the particles to be mu mesons and consider coulomb scattering alone, since the nuclear interactions of the mu meson are very small in comparison with the coulomb interaction. Arguments in support of the overwhelming predominance of mu mesons in the high momentum radiation at sea level will be given later.

Scattering Probability

The relativistic cross-section for coulomb scattering of mesons of spin 1/2 is

$$\sigma = \frac{Z^2 r_o^2 m_o^2}{4 p^2 \beta^2} \left(\frac{1 - \beta^2 \sin^2 \frac{\theta}{2}}{\sin^4 \frac{\theta}{2}} \right) \text{cm}^2 \qquad (8)$$

per unit solid angle, where $r_o = 2.82 \times 10^{-13}$ cm, $m_o = 0.5108$ Mev, and p is in Mev. It can be seen that small angles of

scattering are predominant according to (8) and that for such angles the average number of times that a particle of momentum p will be scattered through an angle θ into the interval $d\theta$ in traversing a plate of scattering material is

$$P(\theta)d\theta = \frac{2k\,d\theta}{\theta^3} \quad , \qquad k = \frac{4\pi Z^2 r_e^2 m_e^2 N t}{p^2\beta^2} \tag{9}$$

where N is the number of scattering centers per cm^3 in the plate, t is its thickness in cm, and Z is its atomic number. In the present experiment the scatterer was about 2 cm of glass for which $Nt = 1.51 \times 10^{23}\ cm^{-2}$.

As was discussed above, the present measurements are concerned with the projections of the angle of deviation on a plane perpendicular to the magnetic field. If φ is the projection of the scattering angle, θ, onto such a plane, then the average number of times that a scattering results in a projected scattering angle, φ, in the interval $d\varphi$ is

$$P(\varphi)d\varphi = k\frac{d\varphi}{\varphi^3} \tag{10}$$

In general the net deflection of a particle passing through the scattering plate will be the result of many small multiple scatterings with a few larger scatterings. As a result of the multiple scatterings, the net angle of scattering will be expected to have a gaussian distribution, although the occasional single and plural large scatterings will cause some deviation from such a distribution. Williams(3) has considered this problem in considerable detail including refinements related to electronic screening and the finite size

of the nucleus. He concludes that the resulting distribution may be very well represented by a broadened gaussian distribution which includes all but the largest scattering angles. The probability that a particle of momentum p be scattered through an angle α into the interval $d\alpha$ now becomes

$$P(p,\alpha)\,d\alpha = \frac{1}{\pi \alpha_m} e^{-\frac{\alpha^2}{\pi \alpha_m^2 d\alpha}} \frac{0.155}{\sqrt{k}} e^{-\frac{\alpha^2}{13.2k}}\, d\alpha \qquad (11)$$

Putting $\beta = v/c = 1$ and introducing numerical values, we find $k = 3.91/p^2$ when p is in Mev. Putting this value into equation (11) we find the probability that a particle of momentum p is scattered through an angle α into the interval $d\alpha$ to be

$$P(p,\alpha)\,d\alpha = 0.0783\,p\, e^{-\left(\frac{\alpha p}{7.24}\right)^2} d\alpha \qquad (12)$$

According to the arguments leading to this result, it is expected to be valid only for angles smaller than $7.33\sqrt{k} = 14.5/p$ when p is in Mev. Beyond this value one must use the inverse cube law of single scattering again although Williams shows that large angle scattering is much reduced by the finite size of the nucleus, an effect that is difficult to calculate exactly. The net result is to make the tail of the probability distribution (12) fall off somewhat more slowly than a pure gaussian distribution. Snyder and Scott (4) have given a detailed analysis of this problem starting with rigorous diffusion equations and have calculated the function that must be used to join the multiple gaussian scattering onto the region of large single scattering. For a 1 Bev particle which

penetrates the scatterer in this experiment, their result agrees with the gaussian used here to within 1% or so at a scattering angle of 5° and predicts about ten times the probability for 10° scattering as does the gaussian. Very large scattering angles are rejected by the counter geometry in this experiment, however, and in any event the total probability of a single scattering through an angle larger than the limiting value 14.5/p is, according to the inverse cube law, 0.018, and according to (12), 0.0025. Hence, (12) predicts 0.016 too few large scatterings and this number is reduced by counter geometry and finite size of the nucleus and selective elimination of those tracks whose position and angle in the chambers make it obvious that scattering has occurred. We are, therefore, safe in assuming fewer than, say, one particle in a hundred is scattered in a way not accounted for by (12).

Probability of Occurrence of Various Fractional Errors in the Momentum Due to Scattering

A particle of momentum p is deflected through an angle θ by the magnetic field in this experiment so that $p = 116.1/\theta$ if p is in Mev and θ is in radians. If the particle is scattered through an angle α in addition, it appears to have a momentum $p' = 116.1/(\alpha + \theta)$. We define the fractional error $w = (p'-p)/p = -(\alpha/\theta)/(1 + \alpha/\theta)$; then the probability that w be between certain limits is the same as the probability that α/θ be between the corresponding ones. We can rewrite the above expression for α/θ in the form $\alpha = -(116.1\ w/p)/(1 + w)$, in which the probability of this value of α is given by (12). Substituting this

form for α into $P(p,\alpha)$ gives an expression containing only w but not p so that the probability of obtaining a certain fractional error in momentum due to scattering is independent of p. To calculate the odds that w lie between certain limits it is easiest to find the values of α corresponding to these limits and evaluate the resulting standard probability integral between assymmetric limits using tabulated values. Most scatterings (35 out of 36) are found to change p by less than 10% of itself, one out of 600 scatterings change p by more than 15% and one out of 10,000 more than 20%. The process is slightly assymmetric so that an apparent decrease in p is somewhat more likely than an apparent increase.

Effect of Scattering on the Momentum Distribution

The differential momentum distribution observed here rises to a peak at about 1 Bev and then falls off as $1/p^n$ at higher momenta, where n is expected to lie between 2 and 3. Since there are many more particles of low momentum one might expect the scattering to result in a net diffusion of observed momenta which would increase the number of particles of apparently high momentum which are observed. To estimate the effect of the scattering on the shape of the distribution we consider a distribution that rises linearly from $p = 0$ to $p = 1$ Bev and falls off as $1/p^3$ for higher momenta. Since positive and negative particles are present in roughly equal numbers we let the distribution be even in p, negative p's meaning negatively charged particles. This convention allows us to include in our analysis the possibility that a particle be scattered in such a way as to suffer an apparent change in sign. It will be more convenient for calculation to transform this momentum

distribution into a distribution of observed angles so we take $x = 1/p = \theta/k$ as a variable proportional to the deflection angle. Then since $dx = -(1/p^2)dp$, the number of particles in the interval dx, $y(x)dx$, becomes

$|x| = 0$ to 1, $y(x) = |x|/2$; $|x| = 1$ to ∞ , $y(x) = 1/|2x^3|$ (13)

When a particle is scattered through an angle α, its new angle will be $\psi = \theta + \alpha$ and new momentum $p' = 1/z$. The probability of such a scattering can be found from (12) to be

$$P(x, z) = \frac{16}{\sqrt{\pi}\,|x|}\, e^{-a^2\left(1-\frac{z}{x}\right)^2} dz \qquad (14)$$

which is the probability that a particle of "angle" x be scattered to an "angle" z in dz. In this expression the quantity, a, is the ratio of the deflection constant of the magnet to the mean scattering angle of the scatterer and has the value 16 in the units used here. If we start with $y(x)dx$ particles in the interval dx and these are scattered with the probability (14) into dz at z, the number that finally appear in dz due to the whole distribution in x is

$$w(z)dz = \left[\int_{-\infty}^{\infty} y(x)dx\, P(x, z)\right] dz \qquad (15)$$

which is the new distribution in "angle" resulting from the scattering of the original one. Our normalization is such that

$$\int_{-\infty}^{\infty} y(x)dx = \int_{-\infty}^{\infty} P(x, z)dz = \int_{-\infty}^{\infty} w(z)dz = 1 \qquad (16)$$

On substituting the expressions(13) and (14) for y(x) and P(x,z) respectively into (15) we get a sum of integrals that

can be reduced partly to standard error functions, and partly to integrals which are readily integrated numerically. When the numerical evaluation is carried out we find the following results for the "scattered" distribution:

p Bev	x	y(x)	p' Bev	z	w(z)
0.1	10	1/2000	0.1	10	1/2000 + 1/4%
.25	4	1/128	.25	4	1/128 + 1/4%
.5	2	1/16	.5	2	1/16 + 1/4%
1.0	1	1/2	1.0	1	1/2 - 9%
2.	0.1	1/20	10.	0.1	1/20 + 0.2%
10.	.5	1/4	2.	.5	1/4 + 0.3%
100.	.01	1/200	100.	.01	1/200 + 0.2%

From these results we conclude that the effect of the scattering on our hypothetical distribution is to decrease the sharp peak about 9% with a slight shift to higher momenta, to increase the number of particles between 0.1 and 0.5 Bev by about 0.3%, and to increase the number between 3 and 100 Bev by about the same percent. Since these changes are all well within the error with which the curve is known from the data, the scattering is completely negligible in its effect on the gross features of the spectrum, provided that one can assume that the scattering is only Coulomb scattering for mu mesons of spin 1/2.

These conclusions result from the very narrow gaussian distribution of scattering angles which is verified experimentally in what follows. It is found that a hypothetical peak of rectangular shape placed at 3 Bev in the distribution and with a width of 1 Bev will be smeared out by the scattering to about two-thirds its original height.

CHAPTER IV

Experimental Errors

In addition to statistical uncertainties in the numbers of particles of various momenta detected in the experiment, the experimental results are affected by distortions in the optical and photographic processes, distortions due to gas flow in the chambers, error in measurement of the magnetic field, modification of the distribution by scattering as discussed above, and error in angle measurements. In addition any assymmetry in the illumination would bias the statistics by accepting more particles from one side of the chambers than from the other. The result would be a bad value for the positive-negative ratio and also an over-emphasis on the low momentum end of the distribution. To avoid these difficulties the direction of the magnetic field was reversed every four hundred pictures (four hundred measureable tracks).

Photographic and optical distortions were found to be completely negligible in comparison with other sources of error in the experiment by examining photographs of sheets of graph paper taken with the recording cameras through the front glass plate as in the actual experiment.

Distortion of the tracks by gas currents in the chambers and the finite width of the tracks were the factors that most seriously limited the accuracy of the measurements. By careful thermal insulation of the magnet and chambers and by reducing the droplet growth time to a minimum for photographability it was possible to obtain very straight thin tracks

whose directions could be measured to better than 0.001 radians. Distortions due to thermal convection currents would occasionally become bad just after an adjustment of the apparatus due to air currents set up in the insulating boxes. It was possible to eliminate the distorted tracks from consideration without biasing the spectrum, however, since one can use some objective criterion to judge straightness of a single track without knowing the energy of the particle responsible for it. In some cases only a short part of the track was distorted and then the long straight portion could be used. It may be that straightness is not a sufficient condition to guarantee lack of distortion; for example, if the axis of a chamber (direction of motion of piston) is not parallel to the axis of the camera, the apparent angle of the track will be altered by the uniform expansion of the gas. Such an effect could give rise to a systematic error favoring particles of one sign. Reversing the magnetic field direction would tend to reduce this effect although calculation of the geometry involved in the present experiment show this possible source of error to be completely negligible. Maps of the distortions present with various arrangements for insulating the cloud chambers make it seem very unlikely that a track be rotated by a flow of gas in the chamber without at the same time being bent out of a straight line.

All of these considerations together with runs of measurements made on the same data by two independent observers lead to an estimated average error in the measurement of angles of

something less than 0.001 radian. Actually most of the tracks of momentum less than 10 Bev were measured only to 0.002 or 0.003 radians, the high energy tracks being remeasured three or four times to at least 0.001 radians.

An experimental estimate of the precision of measurement as limited by these various effects was made in the following way. All of the tracks yielding momenta greater than 10 Bev were remeasured very carefully four independent times with a finer grid than was used for the bulk of the measurements. 206 tracks including 107 no-field tracks were so measured. The variations among the four values were nearly always less than 0.0008 radians so that the averages of the four values are good to probably 0.0005 radians. Comparing these remeasured values with those obtained by the more rapidly done initial measurement gives an estimate of the overall errors of measurement. Of the 206 tracks so treated, 106 gave positive errors, 100 gave negative errors, and the average error was 0.0025 radians. The average error was found to be almost exactly 0.79 times the root mean square error so that the distribution seems gaussian. Of the 107 no-field tracks 53 were apparently positive, 52 negative, and 2 suffered no apparent deflection. The average deflection was 0.0155 radians, the root mean square deflection again confirming the gaussian form of the scattering distribution. If one assumes the no-field measurements to represent a gaussian scattering curve for particles of all the same momentum, the breadth found here corresponds to a momentum of 2.8 Bev whereas the

average momentum of the measured spectrum for the 1530 particles less than 100 Bev is 4.4 Bev and only 15 particles or so remain apparently above 100 Bev. Hence scattering of the particles is found by theoretical estimate and experimental check to have an inconsiderable effect on the momentum distribution except that any sharp peaks which might be present will be smeared out somewhat.

Figs. (5) and (6) show the probable limits within which the observed values of momentum lie for a particle of momentum p. Fig. (5) is derived from the standard deviation found for the coarse measurements and Fig. (6) applies to the stereoscopically remeasured high energy tracks.

Results and Conclusions; Comparison with other Experiments

1547 measureable pairs of photographs were taken in this experiment, 127 of them representing particles of momentum more than 10 Bev. Fig. 7 shows the differential momentum distribution of the particles of momentum less than 10 Bev. Each point represents the number of particles found in a 0.5 Bev interval centered about the momentum plotted as abscissa. Vertical bars indicate the standard deviations of these numbers and the horizontal bars are errors in momentum taken from the curves of Figs. 5 and 6. The dashed curve follows the raw data; the full curve has been corrected for the variation of the aperture of our instrument with momentum. After the correction is applied it is at best difficult to determine the position of the maximum point of the distribution since the instrument is very strongly biased against particles of low

momentum when operated at high magnetic field strengths. An unusual feature of the distribution is the apparent irregularity at about 3.5 Bev which is shown dotted in Fig. 7. Overlapping intervals have been used to plot the low end of the spectrum in order to represent the data in more detail. As a result only half the points shown at the low end are statistically independent. Nevertheless there does seem to be some real indication of a deviation from the main curve at 3.5 Bev.

Table I contains a summary of the salient features of all the surveys of the momentum distribution published to date in which counter-controlled cloud chambers and magnetic fields were used. We have taken the resolving power to be that value of the momentum at which the error in determining the momentum reaches 100%. It can be seen that the experiments varied in some of the details of method as well as in the results. For comparison we have replotted the results the three of the previous surveys in which the largest numbers of measurements were reported. No disagreement outside statistics is found with the results of the other experimenters except at the low end where various amounts of the soft component were included due to different geometries. After normalization to include the same number of particles between about 1 Bev and 10 Bev we find Jones' data seem to agree excellently with the presemt work, the points at 2.5 and 3.5 Bev tending to support the presence of some sort of anomaly in that region. Blackett's data also lie closely on the curve and reveal some kind of bump at about 2.5 Bev as reported in 1937 which is in a dif-

ferent position from the one we find. Hughes' data lie consistently below our curve for momenta above 3 Bev and are consistently high for lower values of p, suggesting that perhaps his detector was biased somewhat in favor of the low momentum particles even though he made mention of a correction similar to the one we applied here. His data suggest a dip in the neighborhood of 3 Bev. In comparing the various sets of data, one should observe that the resolution of the present experiment is roughly twice that of Blackett's. The other authors did not give a detailed error estimate. Our statistical accuracy is about 50% better than previous ones. Figs. 8 and 9 show the differential momentum distributions of positive and negative particles, respectively. Both curves show the same general features although the statistics are not so good as for the total distribution.

In Fig. 10 is plotted the distribution of the excess of positive over negative particles, the full curve representing the data after correction for magnetic biasing. There seems to be a concentration of positive particles around 1.3 Bev with a gradual tailing off toward high momenta. Again the normalized data of previous experiments are replotted and verify in a general way the present results although the poorer statistics and resolving powers of the earlier results wash out the sharp peak to a large extent. In some respects this peak in the excess curve is similar to that obtained by Adams et al.(13) at 30,000 feet above sea level, but in that case it was possible to identify the low energy portion of the

excess as due mostly to protons. Since the peak in the sea-level excess curve occurs at about twice the energy of the peak of the high-altitude curve, it is no longer possible to distinguish protons from mesons by their ionization density. At high altitudes the positive and negative spectra were quite different, the negative spectrum showing practically no peak at 600 Mev where the positive distribution peak occurs. In our instance a smaller difference is found so that a smaller part of the excess is probably due to protons.

Corresponding to the variation of the positive-negative excess with momentum, the ratio of positives to negatives seems to vary with momentum, having a peak at about 1.5 Bev. In Table II are listed the values of the positive-negative ratio computed for 2-Bev intervals centered about the momentum values tabulated.

TABLE II

Center of 2-Bev Momentum Interval	Positive-negative Ratio
1.5 Bev	1.36 ± 0.1
2.5	1.24 ± 0.1
3.5	1.15 ± 0.1

Actually the apparent variation of the positive-negative ratio is not quite outside the statistical variation, but B. G. Owen and J. G. Wilson (18) have recently found an indication of similar behavior with somewhat better statistics. We also agree with Brode (19) who finds the ratio 1.37 ± .04

in a range around 1.5 Bev.

The overallratio of positives to negatives is 1.26 ± 0.06; the ratio for the 127 particles of momentum greater than 10 Bev is 1.2 ± 0.2. When the positive-negative ratio is computed for 1-Bev intervals the peak in the curve appears sharper, the maximum occurring at 1.5 Bev where the ratio becomes 1.6 ± 0.15. At 2 Bev the ratio has fallen to 1.2 ± 0.15.

Throughout this work we have assumed most of our particles to be mu mesons. Electrons are easily ruled out by the experimental evidence that singly occurring electrons of momentum above 0.5 Bev are very rare, particularly at sea level. This results from the very large probability for shower production by fast electrons as mentioned above. Since the fact that nearly all the tracks have about the same ionization density limits us to singly charged particles, we next consider protons. Janossy (14) estimates the fraction of protons among the fast sea level particles to be less than 10% if all the protons are assumed to be of primary origin, if they lose energy by ionization only, and if one assumes about one particle in 500 at sea level is a slow proton as is indicated by experiment. When energy loss due to meson production is considered this estimate becomes 0.1% since meson production energy loss is 100 times ionization loss for fast protons according to the theory of Heitler (15). Since, in addition, many slow protons are known to result from nuclear stars, one may conclude that fast protons are only maybe 0.01% or less of all fast particles at sea level.

Of course one must consider the possibility of pi mesons and other possible singly charged particles, but the 100-times smaller lifetime and the much larger nuclear cross-section make it seem unlikely that the pi/mu ratio be greater than 0.01% though it is probably considerably less in the energy range considered here.

Fig. 11 shows the differential momentum distribution from 10 Bev for all the particles. Plots of the positive and negative particles separately are similar although the statistics are not very good. Since only 127 particles were found in this range, a plot of the positive-negative difference is statistically meaningless.

In order to compare these results with the theory and make various calculations, it is desirable to try to find some simple analytical representation for the cosmic ray momentum distribution. As shown in Fig. 12 the data are well fitted by a distribution of the form $1/p^s$ with $s = 1.8 \pm 0.2$ from 2.5 to 10 Bev and $s = 2.1 \pm 0.3$ from 10 Bev to about 70 Bev. A fairly good fit can also be obtained with an exponential law, e^{-kp}, but at least three different values of k are needed to cover the whole range of momenta. Similarly the integral spectrum can be represented by $1/p^n$ with $n = 1.2 \pm 0.2$ as shown in Fig. 13 in good agreement with the result for the differential spectrum. The upper end of the integral spectrum is somewhat uncertain due to the uncertainty in the number of particles above 100 Bev apparent momentum. Fifteen such particles were found and a $1/p^2$ law for the

differential spectrum when extended to infinite p predicts twelve particles. No significant difference between the analytical behaviors of the positive and negative distributions were found.

In the way of somewhat speculative analysis of the data, it was possible to divide all the particles into two groups; those that occurred at night and those that came in when the sun was above the horizon in Pasadena. By chance the running times of the apparatus at night and during the day gave nearly equal numbers of night time and daytime particles. In Fig. 14 is plotted the momentum distribution of the day particles minus night particles. Although the statistical accuracy is poor, there seems to be some indication of an irregularity favoring 1 Bev particles during the day and 3 Bev ones at night. Perhaps it is not an accident that this 3 Bev anomaly coincides with that of the whole momentum spectrum. Above 10 Bev the same number of particles occurred during the day as at night. In a recent paper K. Dwight (16) gives a calculation of the diurnal variation in primary intensity at the top of the atmosphere due to the combined magnetic fields of the earth and the sun, assuming the sun actually has a permanent field. A rough extrapolation of his results to latitude 33° gives the following expectation. At Pasadena no singly charged particle of momentum less than 7 Bev can hit the earth at the vertical; at the latitude of Chicago and Manchester, England, this minimum energy becomes 2 or 3 Bev. Above 10 Bev no diurnal effect is expected at Pasadena, while between

7 and 10 Bev one expects an effect, the maximum occurring at different times for different momenta. To calculate how rapidly the maximum time varies as the momentum is changed requires considerable numerical work and, in any event, the total variation is not expected to exceed 10%. If the curve drawn roughly in Fig. 14 is to be taken at all seriously, it yields a variation of about 10%. It must be remembered, however, that this curve is presumably for meson secondaries, which makes it seem surprising that any effect should survive at sea level at all. In any event, it might be worth investigating further if the theory can give a reasonably secure prediction so that the results have a bearing on the existence of a permanent solar field.

Instead of regarding measurements of the absorption of cosmic rays under various thicknesses of water and earth as an alternate method for determining the momentum distribution at sea level, we may consider these two experiments as independent observations which can be used to study the rate of energy loss due to ionization by singly charged particles moving faster than the speed for minimum ionization. Rossi (17) finds satisfactory agreement between previous measurements of the sea level momentum distribution and the variation of cosmic ray intensity with depth under ground except for one point at about 20 Bev which seems to indicate too high an energy loss. When the present results are normalized and compared with Rossi's curve, it is found that ionization loss is not sufficient to explain the observed absorption. Here one is getting into the

region where radiative collisions and direct pair production become important sources of energy loss. Calculations are now under way to determine whether these known processes are sufficient to explain the observed absorption results. Some new results of Hazen (unpublished as yet) in a deep salt mine will soon be available for comparison.

REFERENCES

(1) L. F. Kinsler and W. V. Houston, Phys. Rev. (1934), 45, 104

(2) G. Safonov, PhD. Thesis, California Institute of Technology (1949)

(3) E. J. Williams, Proc. Roy. Soc. (1939) ,A 169, 531

(4) H. S. Snyder and W. T. Scott, Phys. Rev. (1949), 76, 220

(5) P. Knnze, Zeits. f. Phys. (1933), 80, 559

(6) C. D. Anderson and S. H. Neddermeyer, Int. Conf. Phys., London, (1934), 177

(7) L. LePrince-Ringuet and J. Crussard, J. de Phys. et Rad. (1937), 8, 207

(8) P.M.S. Blackett and R. B. Brode, Proc. Roy. Soc. (1936), A 154, 573

(9) P.M.S. Blackett, Proc. Roy. Soc. (1937), A 159, 1

(10) H. Jones, Rev. Mod. Phys. (1939), 11, 235

(11) D. J. Hughes, Phys. Rev. (1940), 57, 592

(12) J. G. Wilson, Nature (1946), 158, 415

(13) R. V. Adams, C. D.Anderson, P. E. Lloyd, R. R. Rau, R. C. Saxena, Rev. Mod. Phys. (1948), 20, 334

(14) L. Janossy, Cosmic Rays, Oxford University Press (1948), 146

(15) W. Heitler, Proc. Ir. Ac. (1945), 50, 143

(16) K. Dwight, Phys. Rev. (1950), 78, 40

(17) B. Rossi, Rev. Mod. Phys. (1948), 20, 537

(18) B. G. Owen and J. G. Wilson, Proc. Phys. Soc. London (1949), A 62, 601

(19) R. B. Brode, Phys. Rev. (1949), 76, 468

TABLE I

Summary of Momentum Distribution Surveys

Reference	Resolving Power in Bev	Number of Particles	Peak of Distribution in Bev	Exponent of Power Law	Positive-Negative Ratio	Means of Limiting Electrons
Kunze (5)	3	61	---	---	1	single tracks
Anderson and Neddermeyer (6)	5	78	1.0	-1.7	1.2	single tracks
LePrince-Ringuet and Crussard (7)	20	300	1.0	---	1.7	magnetic cutoff
Blackett and Brode (8); Blackett (9)	20	829	1.0	-1.9	1.2	magnetic cutoff
Jones (10)	10	923	1.0	-1.9	1.3	10 cm lead
Hughes (11)	16	674	1.0	-2.5	1.2	10 cm lead
Wilson (12)	20	424	0.8	-1.8	---	lead
Safonov (2)	40	330	0.9	-2.1	1.5	magnetic cutoff
Glaser	80	1547	---	-1.8 below 10 Bev -2.1 above 10 Bev	1.26±0.06	magnetic cutoff

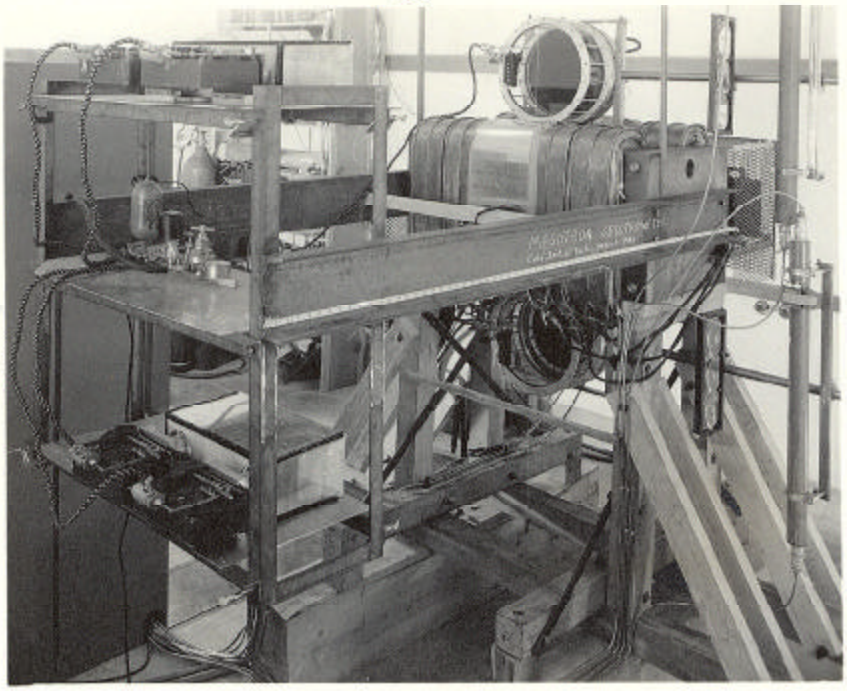

Figure 1a

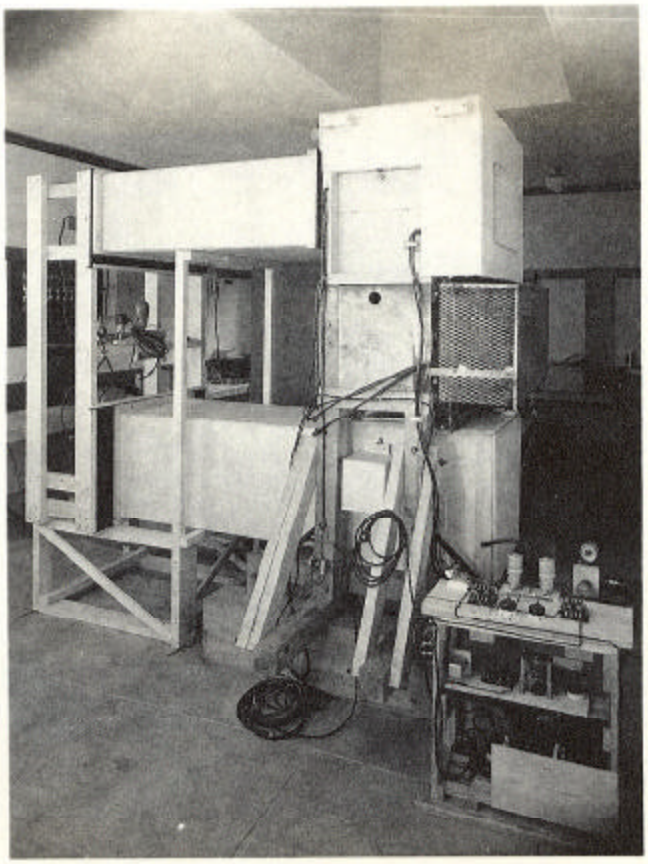

Figure 1b

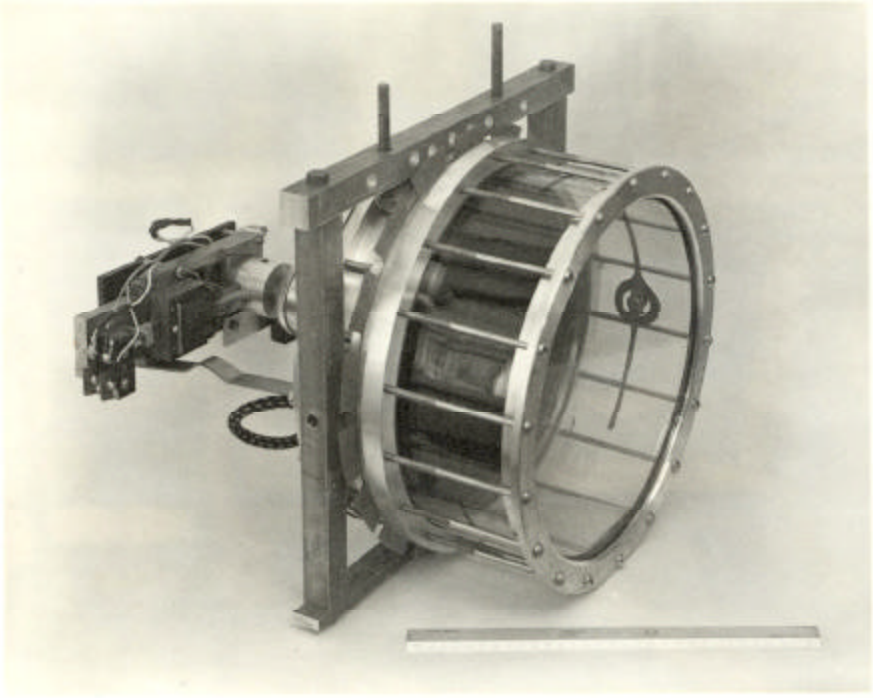

Figure 2a

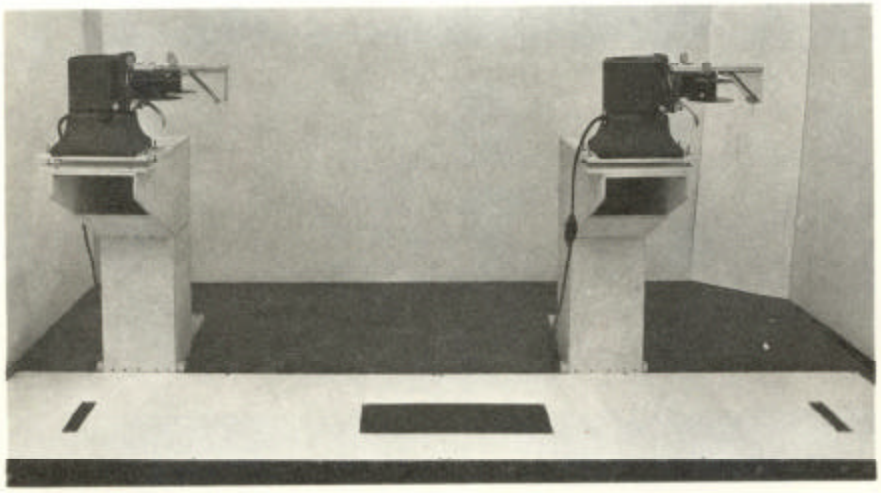

Figure 2b

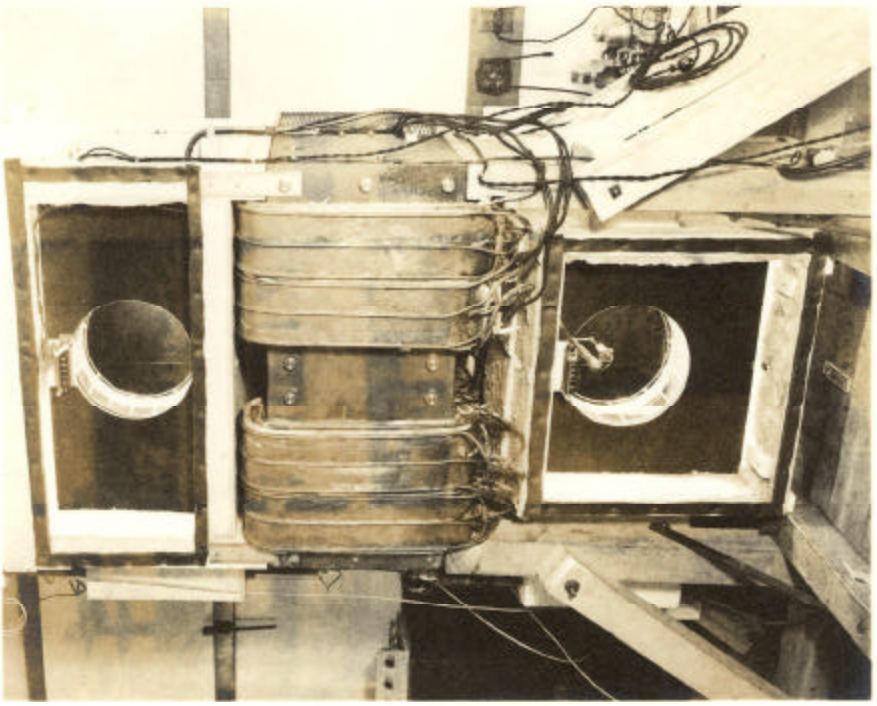

Figure 3b

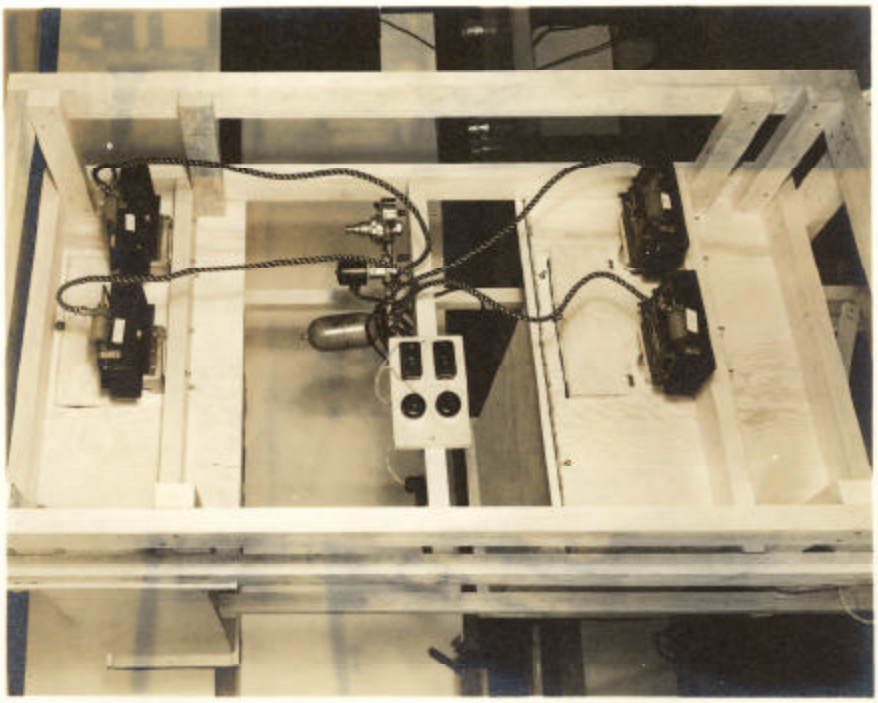

Figure 3a

Figure 4b

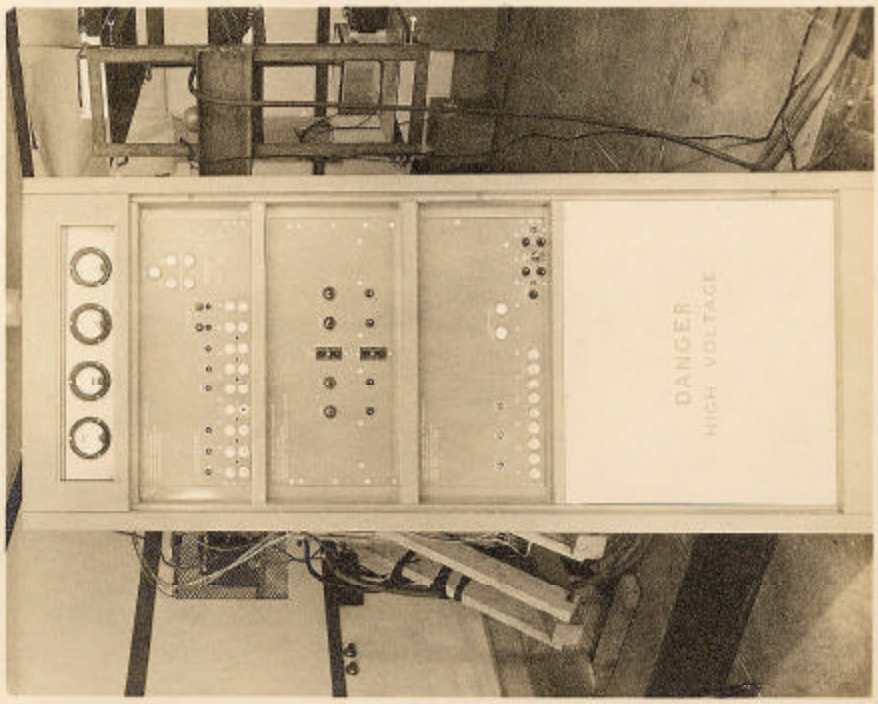

Figure 4a

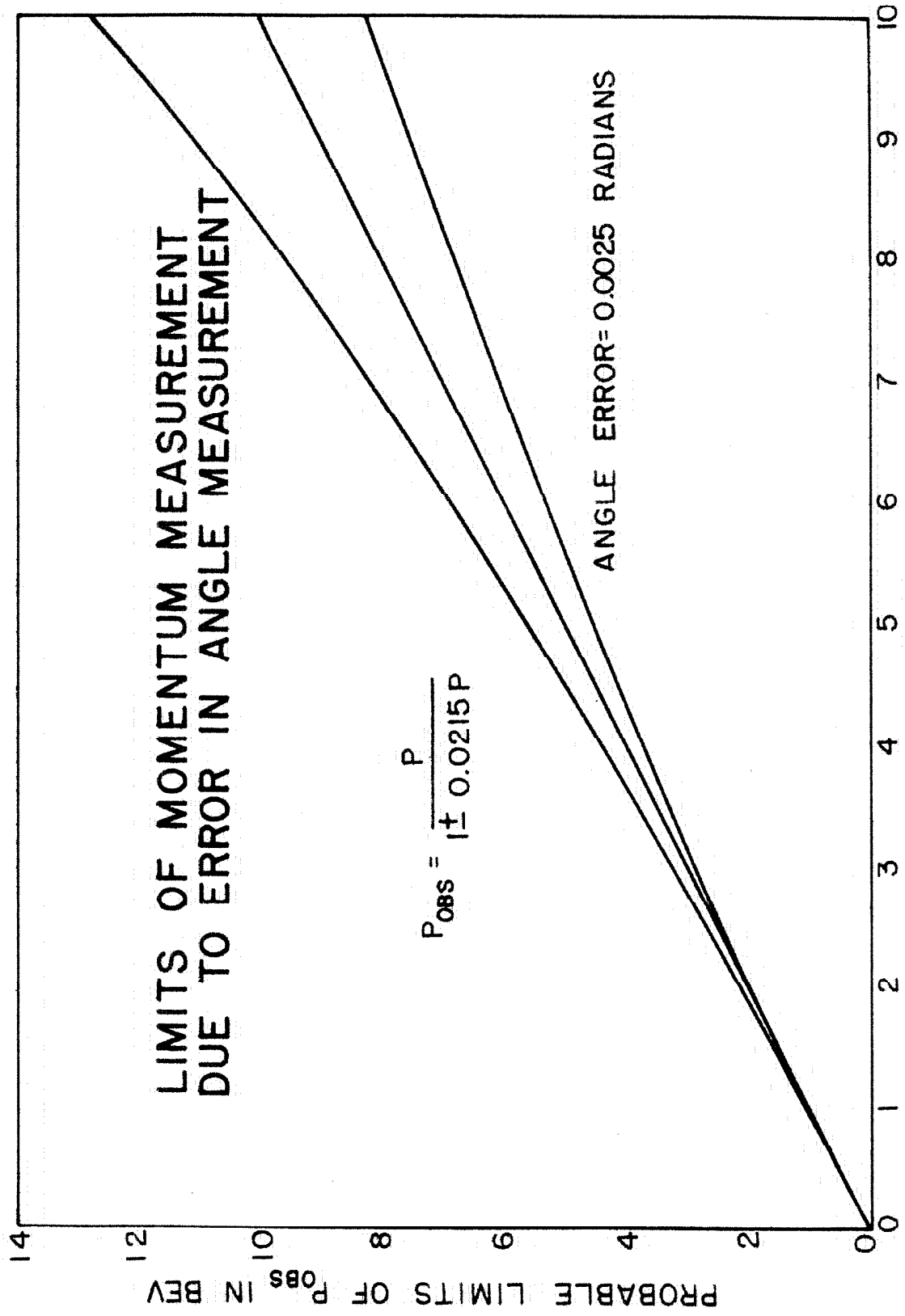
LIMITS OF MOMENTUM MEASUREMENT
DUE TO ERROR IN ANGLE MEASUREMENT
$P_{obs} = \frac{P}{1 \pm 0.0215 P}$
ANGLE ERROR = 0.0025 RADIANS
PROBABLE LIMITS OF P_{obs} IN BEV
P IN BEV
0
2
4
6
8
10
12
14
1
3
5
7
9

Figure 5

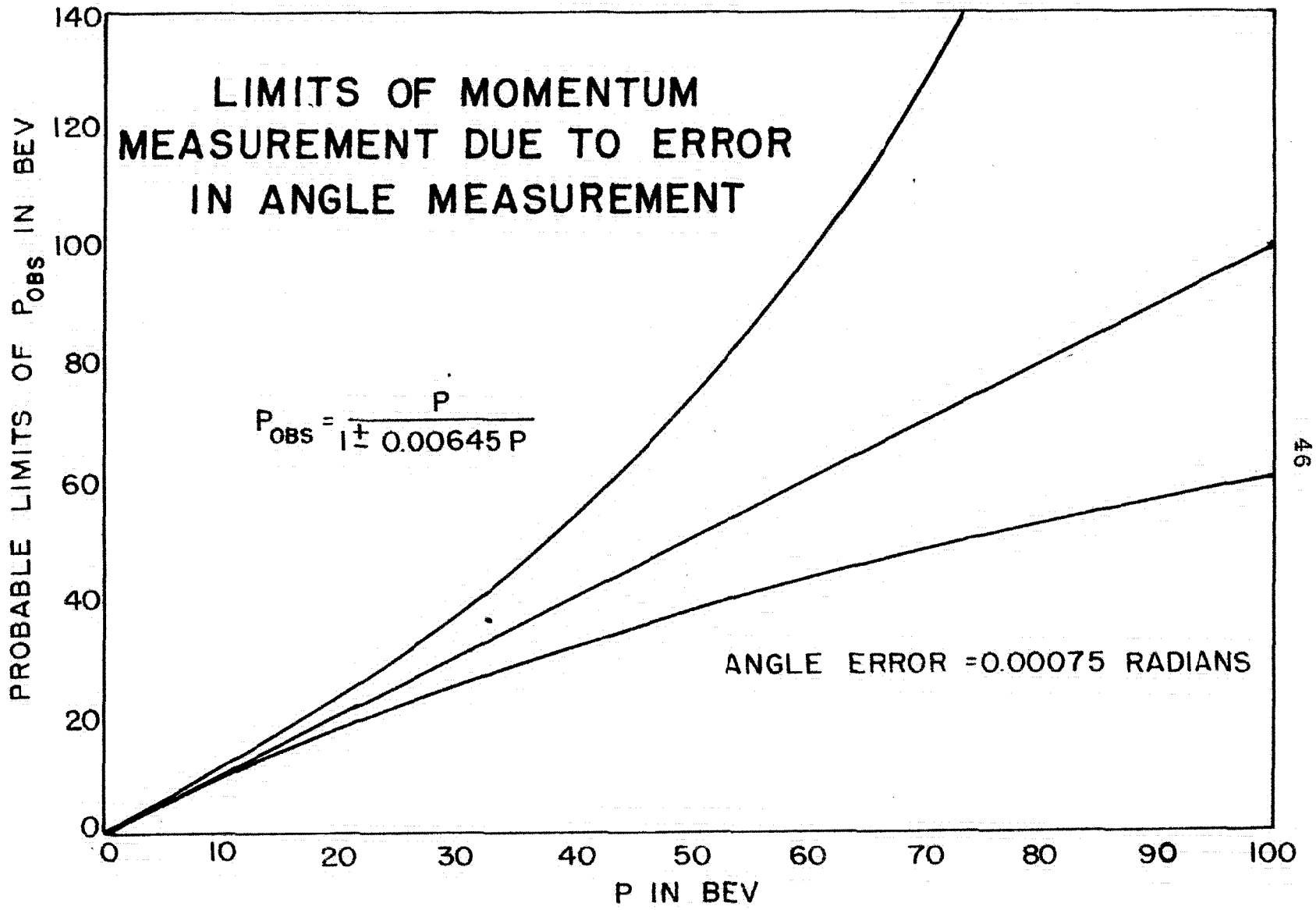
LIMITS OF MOMENTUM
MEASUREMENT DUE TO ERROR
IN ANGLE MEASUREMENT
$P_{OBS} = \frac{P}{1 \pm 0.00645\,P}$
ANGLE ERROR =0.00075 RADIANS
PROBABLE LIMITS OF P_{OBS} IN BEV
P IN BEV
0
20
40
60
80
100
120
140
0
10
20
30
40
50
60
70
80
90
100

Figure 6

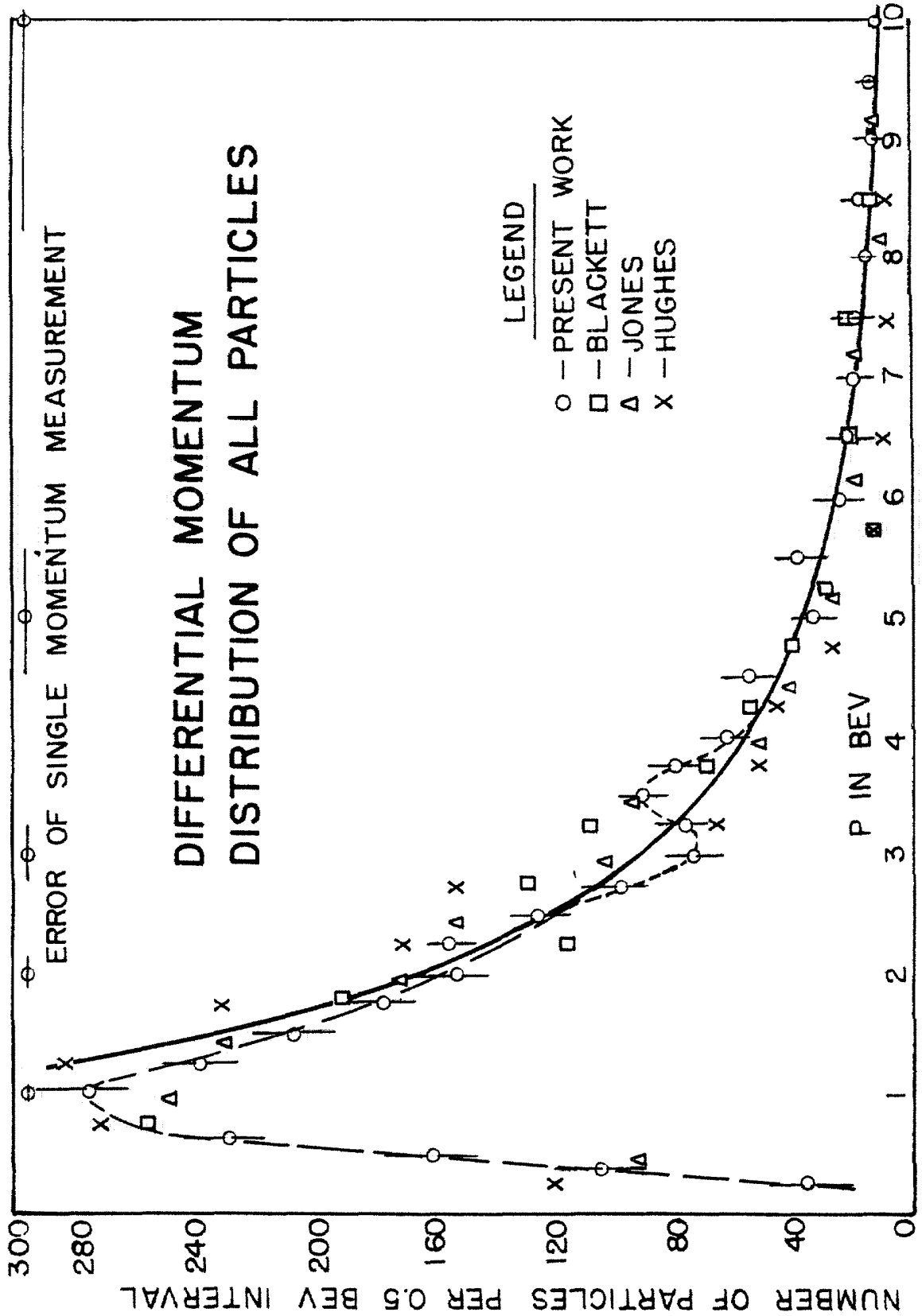
DIFFERENTIAL MOMENTUM
DISTRIBUTION OF ALL PARTICLES
ERROR OF SINGLE MOMENTUM MEASUREMENT
LEGEND
○ — PRESENT WORK
□ — BLACKETT
△ — JONES
X — HUGHES
NUMBER OF PARTICLES PER 0.5 BEV INTERVAL
P IN BEV
0
40
80
120
160
200
240
280
300
1
2
3
4
5
6
7
8
9
10

Figure 7

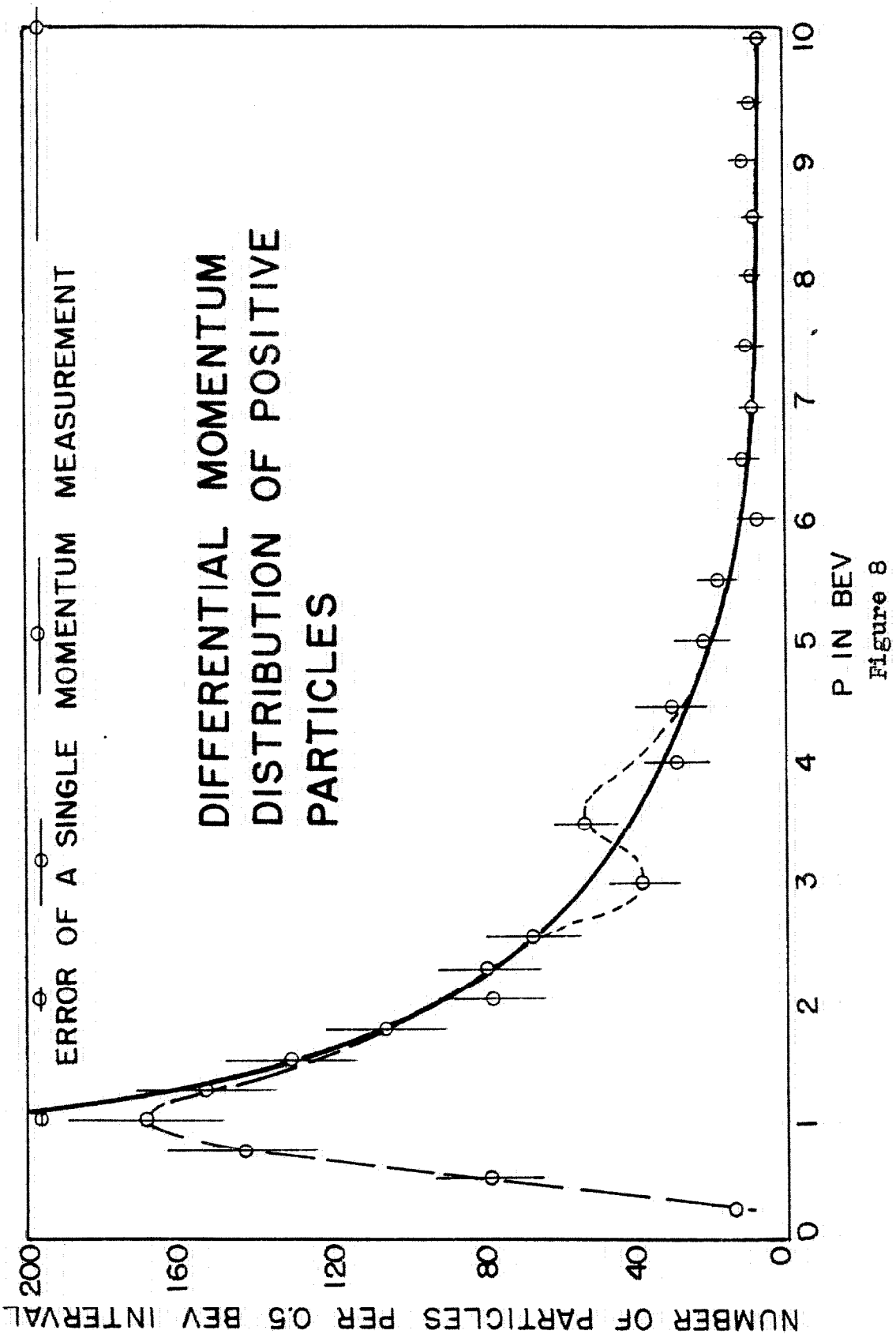
DIFFERENTIAL MOMENTUM
DISTRIBUTION OF POSITIVE
PARTICLES
ERROR OF A SINGLE MOMENTUM MEASUREMENT
NUMBER OF PARTICLES PER 0.5 BEV INTERVAL
0
40
80
120
160
200
0
1
2
3
4
5
6
7
8
9
10
P IN BEV

Figure 8

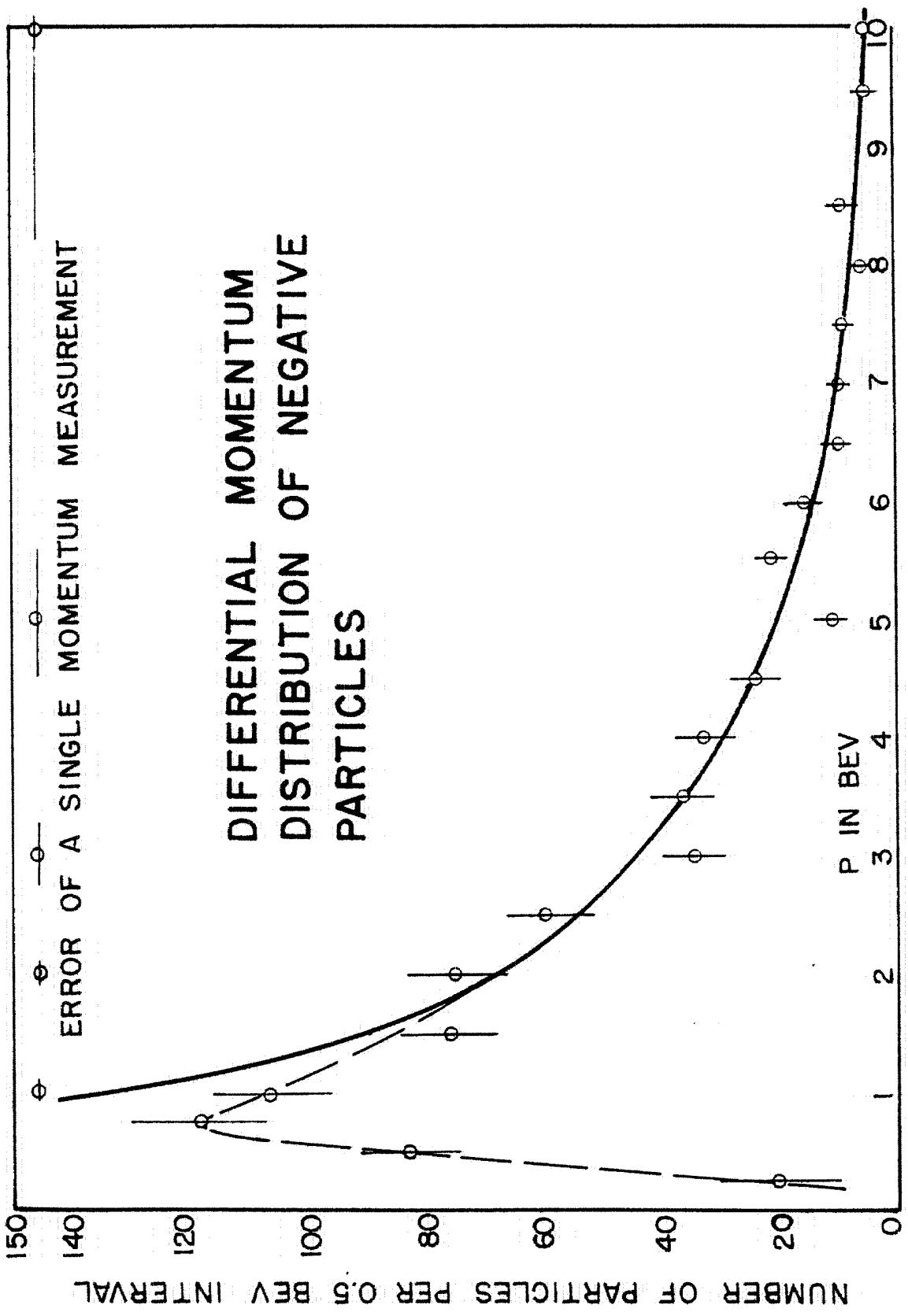
DIFFERENTIAL MOMENTUM
DISTRIBUTION OF NEGATIVE
PARTICLES
ERROR OF A SINGLE MOMENTUM MEASUREMENT
NUMBER OF PARTICLES PER 0.5 BEV INTERVAL
P IN BEV
0
20
40
60
80
100
120
140
150
1
2
3
4
5
6
7
8
9
10

Figure 9

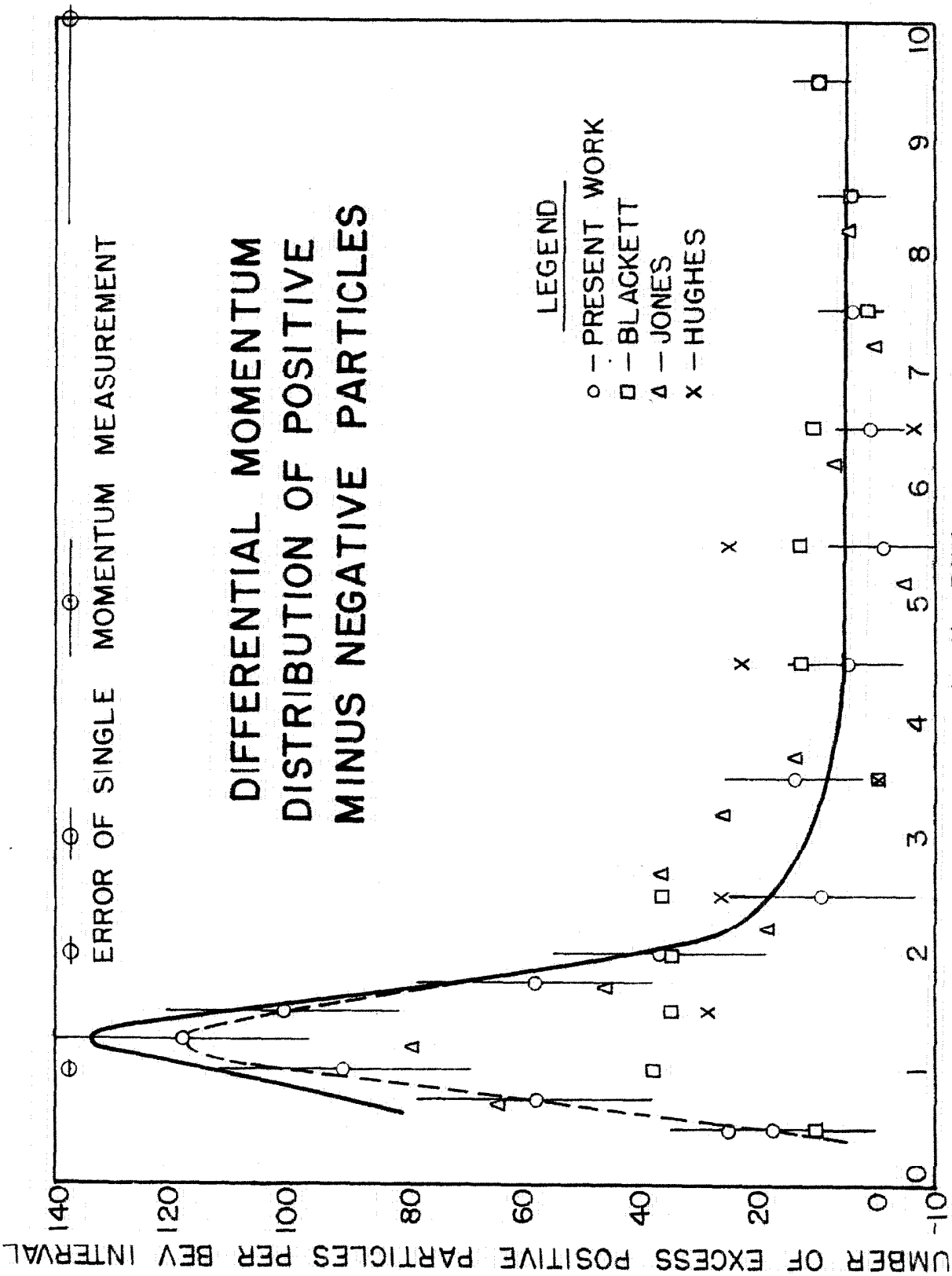
DIFFERENTIAL MOMENTUM
DISTRIBUTION OF POSITIVE
MINUS NEGATIVE PARTICLES
ERROR OF SINGLE MOMENTUM MEASUREMENT
LEGEND
o — PRESENT WORK
□ — BLACKETT
Δ — JONES
x — HUGHES
NUMBER OF EXCESS POSITIVE PARTICLES PER BEV INTERVAL
P IN BEV
-10
0
20
40
60
80
100
120
140
0
1
2
3
4
5
6
7
8
9
10

Figure 10

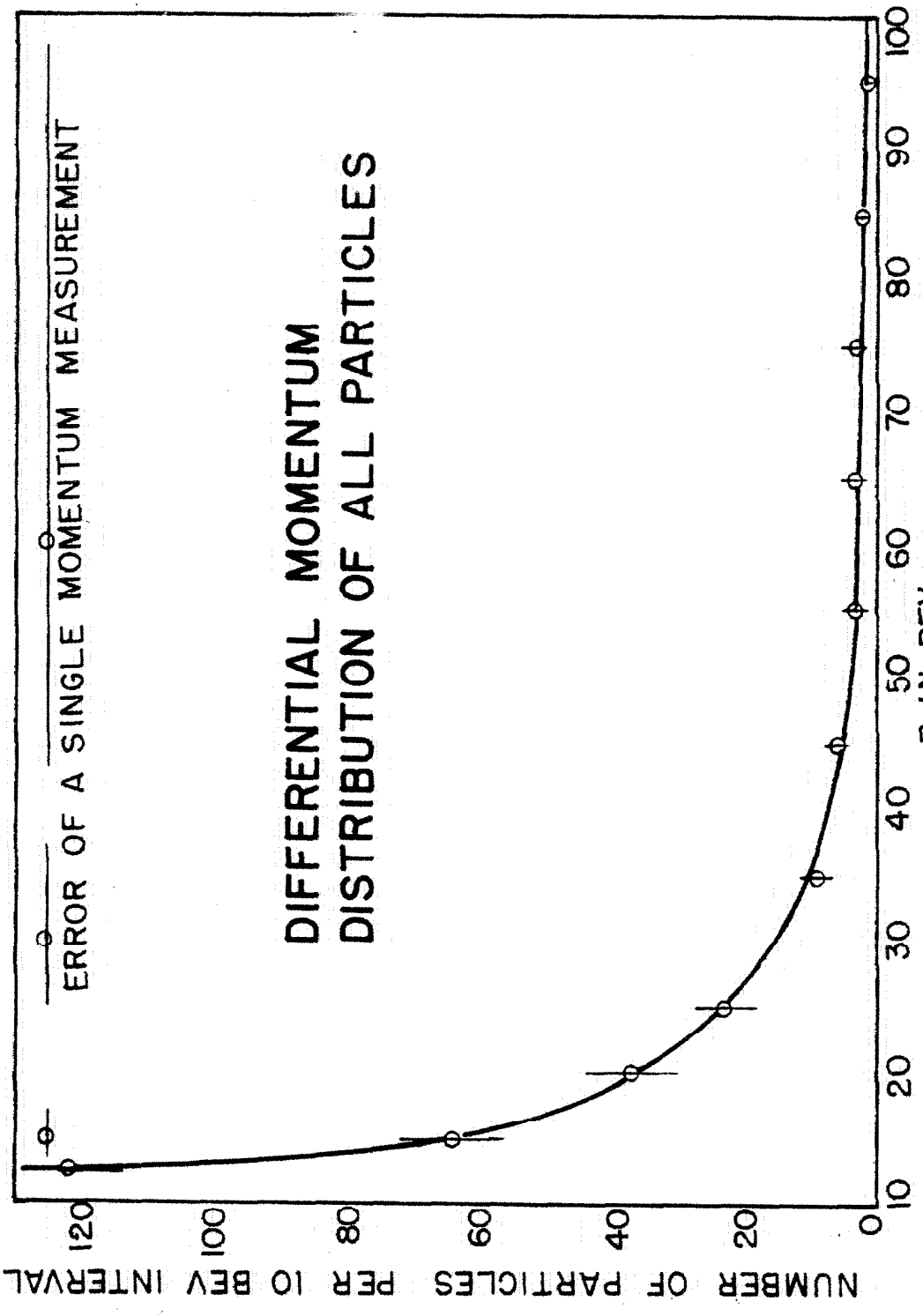
DIFFERENTIAL MOMENTUM
DISTRIBUTION OF ALL PARTICLES
ERROR OF A SINGLE MOMENTUM MEASUREMENT
NUMBER OF PARTICLES PER 10 BEV INTERVAL
0
20
40
60
80
100
120
10
20
30
40
50
60
70
80
90
100
P IN BEV

Figure 11

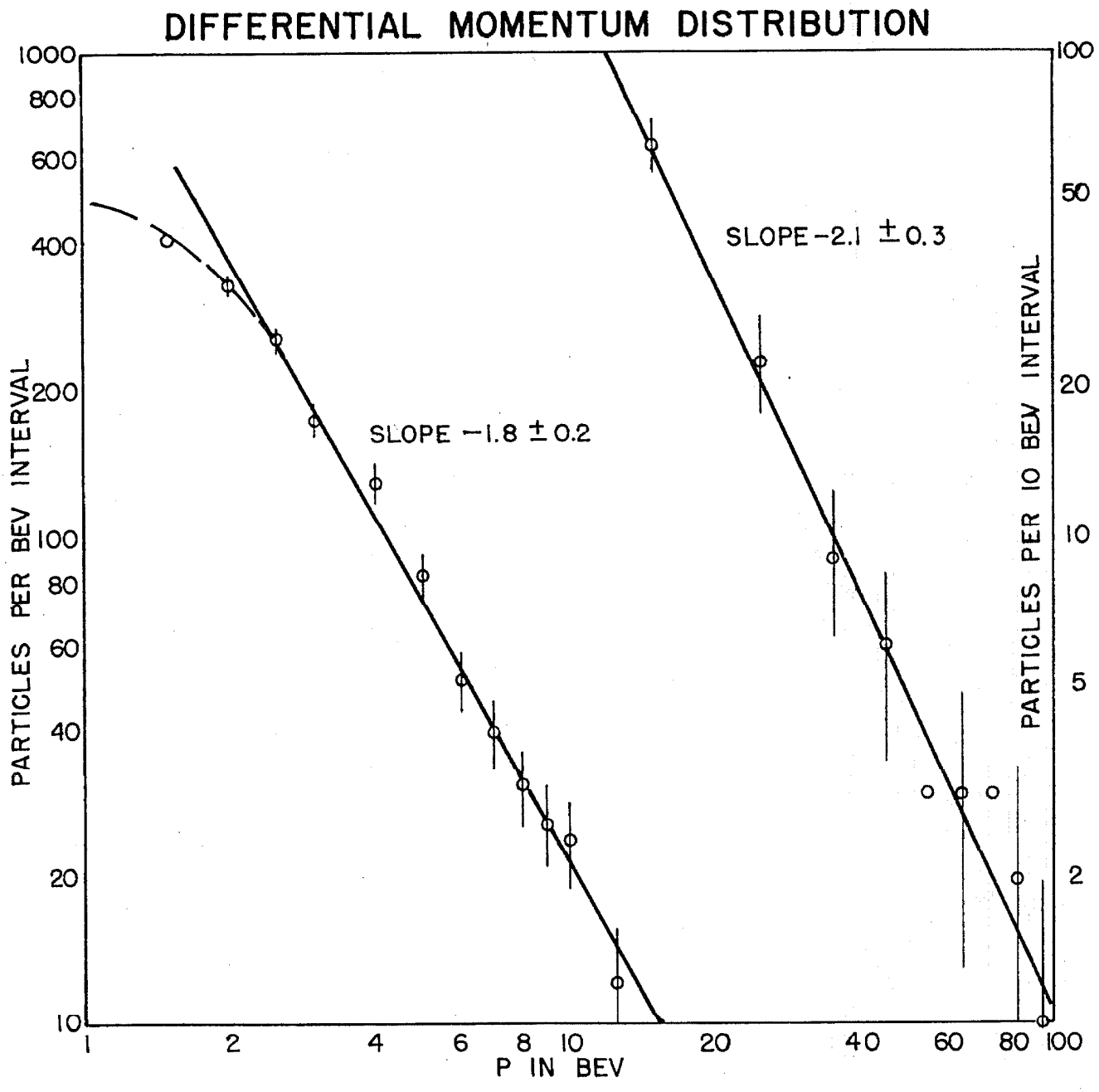
DIFFERENTIAL MOMENTUM DISTRIBUTION
SLOPE −1.8 ± 0.2
SLOPE −2.1 ± 0.3
PARTICLES PER BEV INTERVAL
PARTICLES PER 10 BEV INTERVAL
P IN BEV
1000
800
600
400
200
100
80
60
40
20
10
100
50
20
10
5
2
1
2
4
6
8
10
20
40
60
80
100

Figure 12

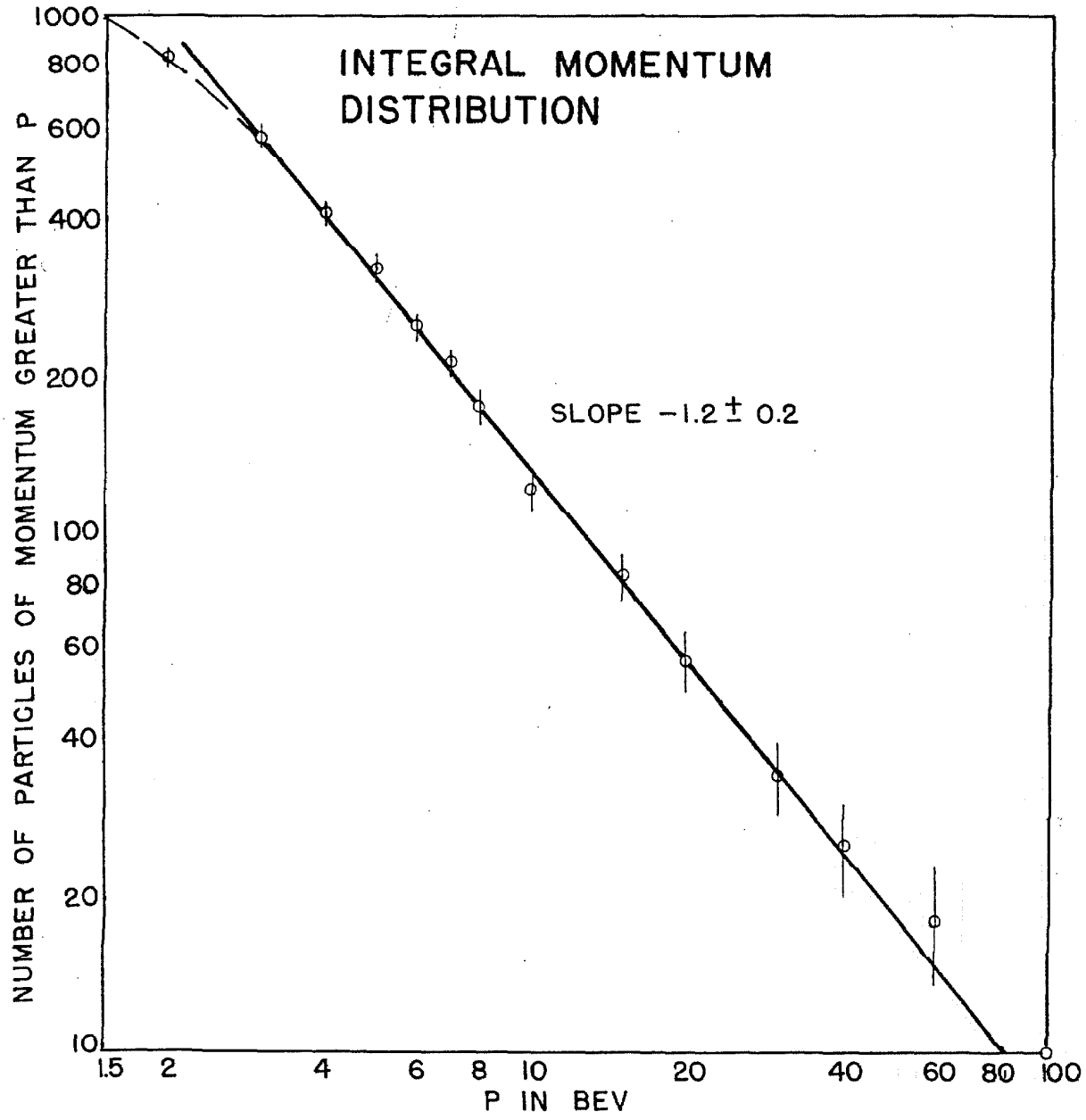
INTEGRAL MOMENTUM
DISTRIBUTION
SLOPE −1.2 ± 0.2
NUMBER OF PARTICLES OF MOMENTUM GREATER THAN P
1000
800
600
400
200
100
80
60
40
20
10
1.5
2
4
6
8
10
20
40
60
80
100
P IN BEV

Figure 13

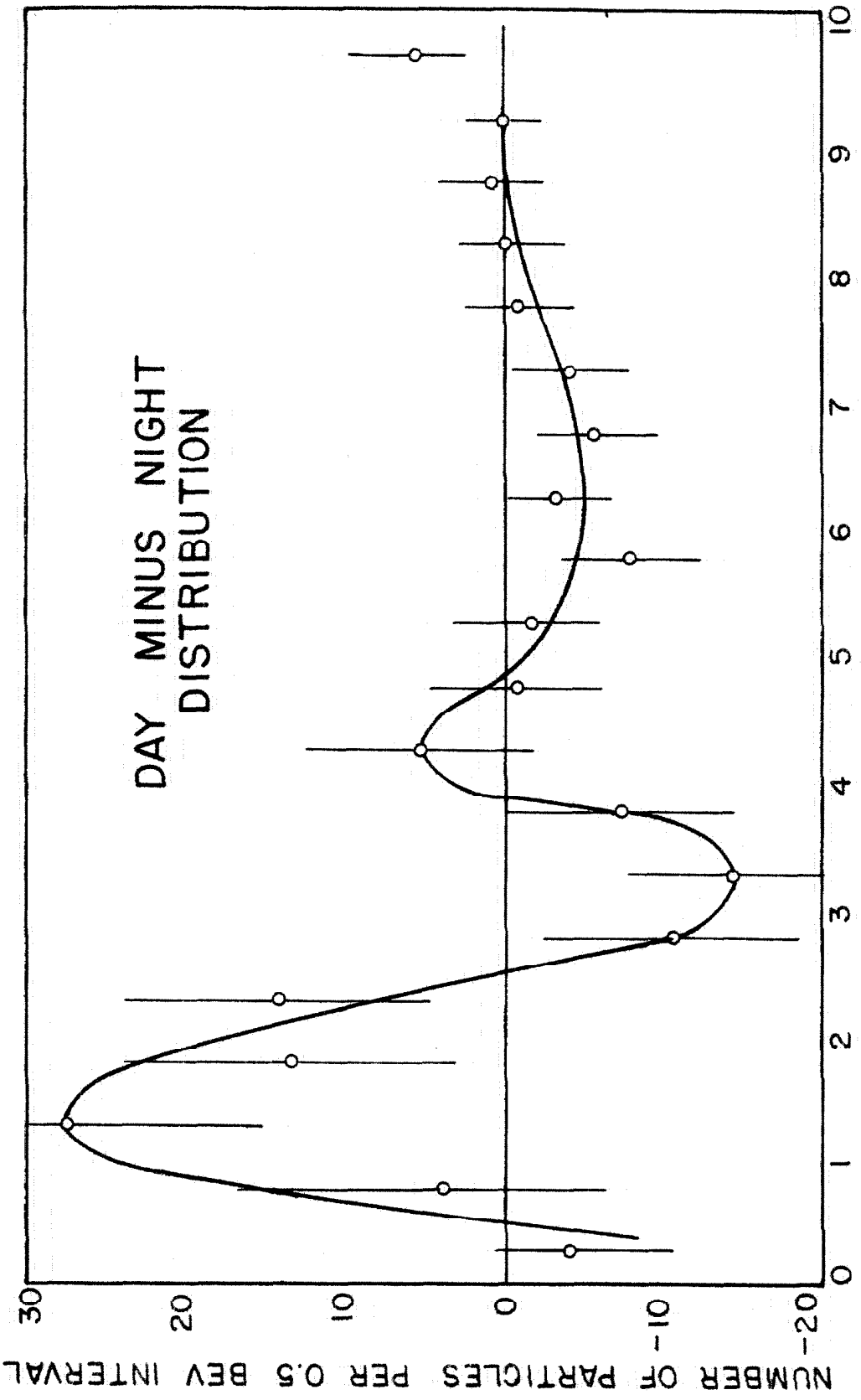
DAY MINUS NIGHT
DISTRIBUTION
NUMBER OF PARTICLES PER 0.5 BEV INTERVAL
30
20
10
0
-10
-20
0
1
2
3
4
5
6
7
8
9
10
P IN BEV

Figure 14